2-Oxopurine Riboside: A Dual Fluorescent Analog and Photosensitizer for RNA/DNA Research

Naishka E. Caldero-Rodríguez,[a] Enrique M. Arpa,[bc] Diego J. Cárdenas,[de] Lara Martínez-Fernández,[be] Steffen Jockusch,[f] Sourav Kanti Seth,[a] Inés Corral,[be] Carlos E. Crespo-Hernández[a]*

[a] Department of Chemistry, Case Western Reserve University, Cleveland, OH 44106

[b] Departamento de Química, Universidad Autónoma de Madrid, c/Francisco Tomás y Valiente 7, Cantoblanco, 28049 Madrid, Spain

[c] Present Address: Linköping University (Linköping, Sweden), Department of Physics, Chemistry and Biology, Office E308

[d] Departamento de Química Orgánica, Universidad Autónoma de Madrid, c/Francisco Tomás y Valiente 7, Cantoblanco, 28049 Madrid, Spain

[e] Institute for Advanced Research in Chemistry (IAdChem), Universidad Autónoma de Madrid, 28049 Madrid, Spain.

[f] Center for Photochemical Sciences, Bowling Green State University, Bowling Green, OH 43403

* Corresponding author; E-mail: carlos.crespo@case.edu; ORCID: 000-0002-3594-0890

KEYWORDS

Fluorescent RNA and DNA Analog, Excited State Dynamics, Electronic Relaxation Mechanism, RNA and DNA Photosensitizer Analog, Singlet Oxygen

Abstract

There is a great interest in developing suitable nucleoside analogs exhibiting high fluorescence and triplet yields to investigate the structure, dynamics, and binding properties of nucleic acids and promote selective photosensitized damage to DNA/RNA, respectively. In this study, steady-state, laser flash photolysis, time-resolved IR luminescence, and femtosecond broadband transient absorption spectroscopies are combined with quantum chemical calculations to elucidate the excited state dynamics of 2-oxopurine riboside in aqueous solution and to investigate its prospective use as a fluorescent or photosensitizer analog. The Franck-Condon population in the S_1 ($\pi\pi^*$) state decays through a combination of solvent and conformational relaxation to its minimum in 1.9 ps. The population trapped in the $^1\pi\pi^*$ minimum bifurcates to either fluoresce or intersystem cross to the triplet manifold within ca. 5 ns, while another fraction of the population decays nonradiatively to the ground state. It is demonstrated that 2-oxopurine riboside exhibits both high fluorescent (48%) and significant triplet (between 10% and 52%) yields, leading to a yield of singlet oxygen generation of 10%, making this nucleoside analog a dual fluorescent and photosensitizer analog for DNA and RNA research.

Introduction

Nucleosides are considered the basic building blocks of DNA and RNA and, subsequently, essential in nearly all biological processes.[1] Canonical nucleosides, which are naturally nonfluorescent,[2 3 4] can be modified by simple structural changes, maintaining a small molecular size, and hydrogen-bonding interactions to enhance their emissive properties and be suitable for the study of biological systems.[5] This type of fluorescent nucleoside analogs is known as isomorphic and is an indispensable tool for understanding nucleic acid structures and interactions at the molecular level.[6 7] For instance, fluorescent nucleoside analogs are extensively developed for DNA and RNA site-specific labeling applications,[8 9] where they replace a canonical nucleoside in a particular position and report conformational and environmental changes through modifications in their fluorescent properties such as lifetime, emission maximum, and quantum yield.[10]

Similarly, nucleoside analogs are currently being developed for photodynamic therapy applications.[11 12 13 14 15 16 17 18] Here, minor chemical modifications are thought to minimize changes to the DNA and RNA structures and maximize hydrogen bonding and base stacking interactions. Either as fluorescent analogs or as photodynamic therapy agents, their photophysical and photodynamical properties must be investigated first to understand and interpret changes in their intrinsic fluorescence parameters[6] or photochemical reaction pathways[11 19 20 21] when incorporated in DNA/RNA polymers.

2-Oxopurine riboside (2oxoP-r) contains a carbonyl group at the C2 position of the purine chromophore. 2OxoP-r is a constitutional isomer of inosine (i.e., hypoxanthine riboside), which has been reported to form alternative base pairs with canonical nucleobases such as adenine and cytosine.[22 23] Computational work done by Corral and coworkers[24] predicts a significant redshift

in the absorption spectrum of the N9H 2-oxopurine tautomer compared to the natural nucleobases, allowing its selective excitation when incorporated in RNA or DNA. Although the synthesis of 2oxoP-r is known,[25, 26] and it has been shown to be significantly fluorescent when incorporated in oligonucleotides,[27, 28] its excited state dynamics and relaxation mechanism have not been investigated.

In this work, we use steady-state absorption and emission spectroscopies and femtosecond broadband transient absorption spectroscopy to investigate the photophysics and excited state dynamics of 2oxoP-r in aqueous solution at pH 6. The experimental work is combined with the quantum chemical calculations recently reported by Corral and coworkers[24] for the N9H tautomer of 2-oxopurine and with new transient absorption spectra simulations presented herein to unravel its primary electronic relaxation mechanism and assist in the interpretation of the experimental results. It is demonstrated that 2oxoP-r is a dual fluorescent and photosensitizer nucleoside analog that can be readily applied for DNA/RNA research.

Experimental and Computational Details

The phosphate buffer with a total phosphate concentration of 16 mM was freshly prepared using monopotassium and dipotassium phosphate salts in ultrapure water and adjusted to pH 6.0 using a 0.1 M sodium hydroxide (NaOH) solution.

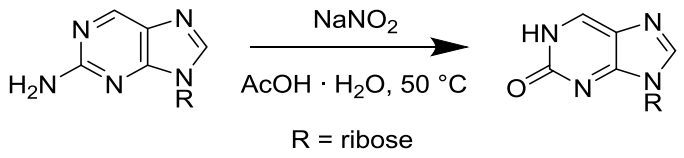

Scheme 1. Synthesis of 2-oxopurine riboside (2oxoP-r). This synthesis was performed by modifying the synthesis of substituted xanthines in ref 29.

Synthesis of 2oxoP-r

2-oxopurine riboside (2oxoP-r) was synthesized following a modified protocol reported previously (Scheme 1).[29] To a stirred solution of 2-aminopurine riboside (250 mg, 0.94 mmol) in a mixture of acetic acid (2.7 mL) and water (0.3 mL) at 50 °C (132 °F), a solution of sodium nitrite (258.2 mg, 3.74 mmol, in 1 mL of water) is added dropwise for 15 minutes. The reaction mixture is left under stirring and heating for an additional 60 minutes. The reaction is then quenched by cooling and eliminating the solvent on a rotary evaporator. The mixture is redissolved in 10 mL of DMSO, filtered, and evaporated under reduced pressure to afford 2oxoP-r as an orange solid. Further water elimination by oven-drying is discouraged to prevent thermal instability and decomposition.

2oxoP-r was characterized by ultrahigh resolution mass spectroscopy (maXis™ UHR-TOF), NMR spectroscopy (Figure S1), and Fourier-transform infrared (FT-IR) spectroscopy (Figure S2). FT-IR was measured using a JASCO ATR-FTIR-4600 spectrometer. MAXIS-MS Calculated: 291.0705 $[M+Na]^+$, Found: 291.0700. ^{1}H NMR (500 MHz, D_2O) δ: 8.50 (s, 1H), 8.43 (s, 1H), 5.96 (d, J = 5.5 Hz, 1H), 4.75 (t, J = 5.5 Hz, 1H), 4.42 (t, J = 4.8 Hz, 1H), 4.24 (q, J = 4 Hz, 1H), 3.80 - 3.92 (m, 2H), 2.72 (DMSO),[30 31] 1.96 (Acetic acid).[30 31] FT-IR (neat), ν_{max} cm^{-1}: 3265 (w), 2918 (w), 1650 (m), 1569 (m), 1405 (m), 1104 (w), 1015 (s). The assignment of these bands was supported by the FT-IR spectrum of 2oxoP-r calculated in vacuum using density functional theory (DFT) at the B3LYP/6-311++G(d,p) level of theory with Gaussian 16 suite of programs.[32] The FT-IR spectrum presents a broad band at 3265 cm^{-1}, corresponding to the O-H stretch in the ribose and the N-H and C-H stretching signals of the purine chromophore. The band at 2918 cm^{-1} corresponds to the C-H stretch of the ribose. This spectrum also presents the distinctive band of the conjugated carbonyl at 1650 cm^{-1}, followed by the C=C stretching at 1569

cm^{-1}. Bands at 1405 and 1104 cm^{-1} were assigned to the C-C aromatic and C-N stretching, respectively. A strong band that corresponds to the C-O stretch in the ribose is observed at 1015 cm^{-1}.

Steady-state measurements

Steady-state absorption spectroscopy was performed using a Cary 300 Bio spectrophotometer using a 300 nm/min scan rate, a data interval of 0.5 nm, and an average time of 0.1 seconds. Steady-state emission spectroscopy was performed using a Cary Eclipse spectrofluorometer using a scan rate of 120 nm/min, 5 nm slit widths, and a PMT voltage of 400 V. The fluorescence quantum yield measurements were recorded on a ISS-PC1 photon-counting spectrofluorometer using 4 nm slit widths, step size of 1 nm, and 20 iterations. A quinine sulfate in 0.05 M sulfuric acid (H_2SO_4) solution was used as the standard.[33] An average of five measurements was reported. These measurements were obtained using samples with an optical density of < 0.1 at the excitation wavelength, 308 nm, to minimize inner filter effects.

Femtosecond broadband transient absorption spectroscopy

The excited state relaxation mechanism of 2oxoP-r was elucidated using broadband transient absorption spectroscopy. The transient absorption setup used has been described in detail in previous publications.[34] [35] Briefly, a Ti:Sapphire oscillator (Vitesse, Coherent) seeds a regenerative amplifier (Libra-HE, Coherent) and produces 100 fs pulses with a 1kHz repetition rate (800 nm). The laser output seeds an optical parametric amplifier (TOPAS, Quantronix/light conversion), which was tuned to the excitation wavelength, 308 nm. A translating 2 mm CaF_2 crystal generates the white light continuum for probing, with a spectral range from 320 to 700 nm. Freshly prepared samples in 2 mm path length fused silica cells were used for the transient absorption measurements, where the solutions were continuously stirred by a Teflon-coated

magnetic stir bar. No photodegradation was observed in the solutions after transient absorption measurements (Figure S3). The data collection was performed using a homemade software, LabView program, while the data analysis was done using the Glotaran graphical user interface to the R-package TIMP software.[36]

Quantum chemical calculations

The Excited State Absorption Spectra were simulated on top of the CASSCF geometries reported in ref 24 using the same protocol, i.e., MS-CASPT2/SA-CASSCF(14,11)/6-31G(d,p), after increasing the number of roots up to 10.[37 38 39 40] The IPEA shift was set to 0.0, and an IMAG shift of 0.3 was used.[41 42] The calculations were done with OpenMolcas.[43]

Laser flash photolysis

Laser flash photolysis experiments were used to characterize the triplet state of 2oxoP-r. These experiments employed pulses generated by a Spectra Physics GCR-150-30 Nd:YAG laser with excitation wavelengths of 266 nm (5 ns pulse width) and a computer controlled system that has been described in detail elsewhere.[44] Experiments were performed in a 1 cm optical cell with an absorbance at the excitation wavelength of ~0.3 in phosphate buffer (pH 6) and in ethanol. Deoxygenated solutions were prepared by purging with argon gas for at least 20 minutes.

Singlet oxygen quantum yields

Time-resolved luminescence spectroscopy was used to determine the singlet oxygen quantum yields for 2oxoP-r. A Spectra Physics GCR-150-30 Nd:YAG laser (266 nm, 5 ns pulse width) was used as the excitation source. Singlet oxygen phosphorescent decay traces were collected at 1270 nm using a modified Fluorolog-3 spectrometer (HORIBA, Jobin Yvon), with a near-IR sensitive photomultiplier tube (H10330A-45, Hamamatsu) as detector. The decay traces were stored on a digital oscilloscope (TDS 360, Tektronics). Solutions of 2oxoP-r and the

phenalenone standard were prepared in phosphate-buffered D_2O (pH 6) and in ethanol at an optical density of 0.3 at the excitation wavelength in 1 cm path length quartz cuvettes. The O_2-saturated solutions were bubbled with O_2 gas for at least 20 min prior to testing. Degradation of the samples was determined to be less than 3% over the course of the experiments based on their steady-state absorption spectra. The quantum yields were determined in back-to-back luminescence experiments of 2oxoP-r and phenalenone solutions under the same conditions, using the reported yield of $^1O_2$ generated by phenalenone as a standard ($\Phi_\Delta = 0.98$).[45]

Results

Steady-state spectroscopy

Previous experimental[28, 46] and theoretical[47] studies have shown that the 2-oxopurine in aqueous solution primarily exists in the keto form. Three pK_a values of 1.69, 8.43, and 11.90 have been reported for 2-oxopurine,[48] and a pK_a of 9.28 has been observed for 9-methyl-2-hydroxypurine.[49] The Henderson-Hasselbach equation (1):[50]

$$pH = pKa + log\frac{[A-]}{[HA]} \qquad (1)$$

was used to determine that 2oxoP-r exists as the neutral species (>99%) in phosphate buffer at pH 6, and thus, we will only consider the keto neutral form of 2oxoP-r in this investigation.

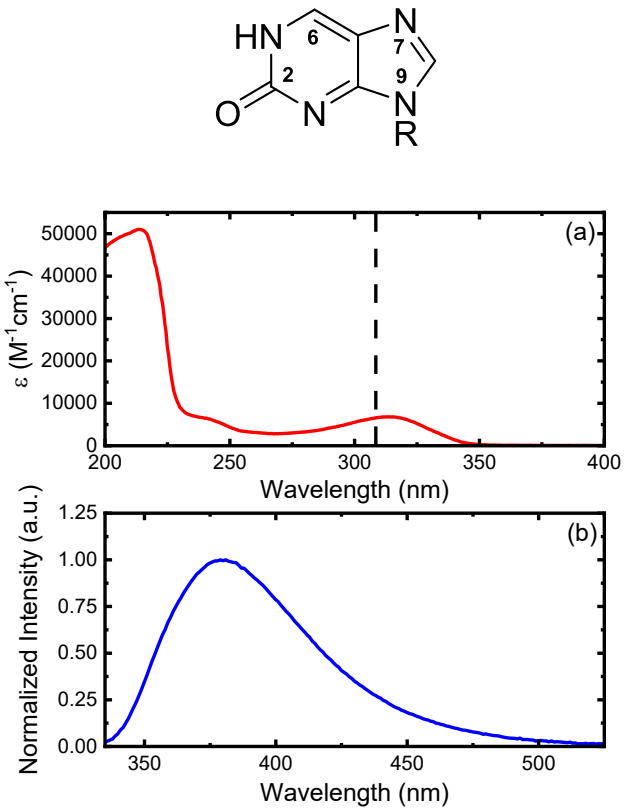

Figure 1. Top: Structure and standard ring numbering of 2oxoP-r (R = ribose). (a) Molar absorption (ε, red) and (b) normalized emission (blue, λ_{exc} = 313 nm) spectra of 2oxoP-r in phosphate buffer pH 6. The molar absorption coefficients were reported by ref. 25 for 9-(β-D-Ribofuranosyl)-2-hydroxypurine in aqueous solution at pH 7. The dashed line indicates the excitation wavelength used for transient absorption measurements (308 nm).

Figure 1 shows the normalized absorption (Figure 1a) and emission (Figure 1b) spectra of 2oxoP-r in phosphate buffer at pH 6. 2OxoP-r contains three absorption bands centered at 313, 240, and 214 nm, where the maximum of the lowest energy absorption band has a molar absorption of 6.8×10^3 M^{-1} cm^{-1} and extends to ca. 350 nm.[25] The two lowest-lying absorption bands agree with calculations performed for the N9H 2-oxopurine tautomer at the CASPT2 level of theory.[24]

It should be noted that the lowest energy band maximum of 2oxoP-r is redshifted by only ca. 10 nm compared to 2AP,[35, 51] which enables its excitation at longer wavelengths into the UVA region. 2OxoP-r also exhibits a single broad emission band with a maximum at 380 nm (Figure 1b),[26, 28] which extends over to 525 nm and is assigned to fluorescence emission due to the relatively small Stokes' shift of 5,325 cm^{-1} (Figure S4). The transition energy between the lowest vibrational levels of the ground state and the first excited singlet state ($E_{0,0}$) was obtained from the intersection point between the normalized excitation and emission spectra (Figure S4), getting a value of (29,167 ± 85) cm^{-1} or 3.62 eV, comparable to the energy calculated (3.40 eV) for the S_1 state of the N9H 2-oxopurine tautomer in vacuum by Corral and coworkers.[24] A fluorescence quantum yield (λ_{exc} = 308 nm) of 0.48 ± 0.04 was measured for 2oxoP-r in phosphate buffer at pH 6, which is only ca. 30% lower than the fluorescence yield reported for 2AP in phosphate buffer at pH 7.[35]

Femtosecond broadband transient absorption spectroscopy

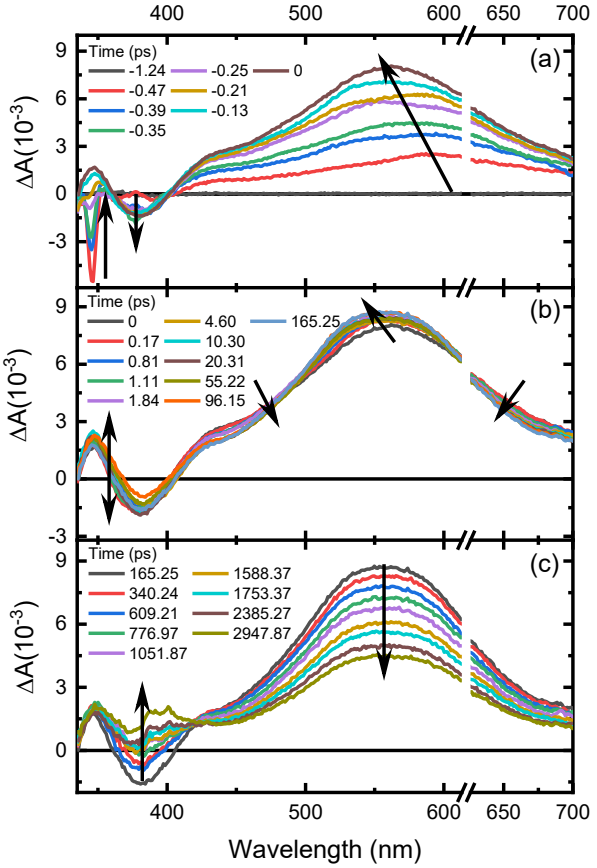

Figure 2. Transient absorption spectra of 2oxoP-r in phosphate buffer pH 6 upon excitation with 308 nm. Time zero was defined at the maximum amplitude of the stimulated emission band of 2oxoP-r at 380 nm. The breaks mask the scattering of the pump beam that reaches the detectors. The stimulated Raman emission band of the solvent is observed around 345 nm in panel a.

Femtosecond transient absorption experiments were performed to elucidate the excited state relaxation mechanism of 2oxoP-r. Figure 2 shows the transient absorption spectra in phosphate buffer at pH 6 following excitation at 308 nm. Excitation of 2oxoP-r results in the observation of a broad transient absorption band with a maximum at 590 nm that blue shifts to 560 nm within the cross-correlation of the pump and probe beams (Figure 2a), a shoulder at ca. 430

nm, an absorption depression around 380 nm, and a smaller band at 345 nm. The spectral depression is assigned to stimulated emission occurring in that spectral region, which agrees with the steady-state emission spectrum of 2oxoP-r presented in Figure 1b. The transient absorption band centered at 560 nm continues to blueshift to ca. 555 nm and narrows with a simultaneous increase in intensity, while a slight redshift is observed for the spectral feature at 380 and the band at 345 nm slightly increases and decreases (Figure 2b). After that, the transient band at 555 nm decreases in amplitude, with a simultaneous increase in intensity in the spectral region between 350 and 420 nm, forming a new band in the latter region and an apparent isosbestic point at ca. 420 nm. The transient absorption bands persist for longer than the time delay of 3 ns used in this study (Figure 2c).

Figure 3 depicts the global and target analyses of the transient absorption data of 2oxoP-r. The spectral region from 350 to 700 nm was satisfactorily analyzed using a three-component sequential kinetic model (Figure 3a). Lifetimes of 1.9 ± 0.4 ps and 5 ± 2 ns were extracted for 2oxoP-r. A third lifetime (>> 5 ns, see below) was required to fit the residual transient absorption spectra in Figure 2c, associated with the blue EADS in Figure 3b.

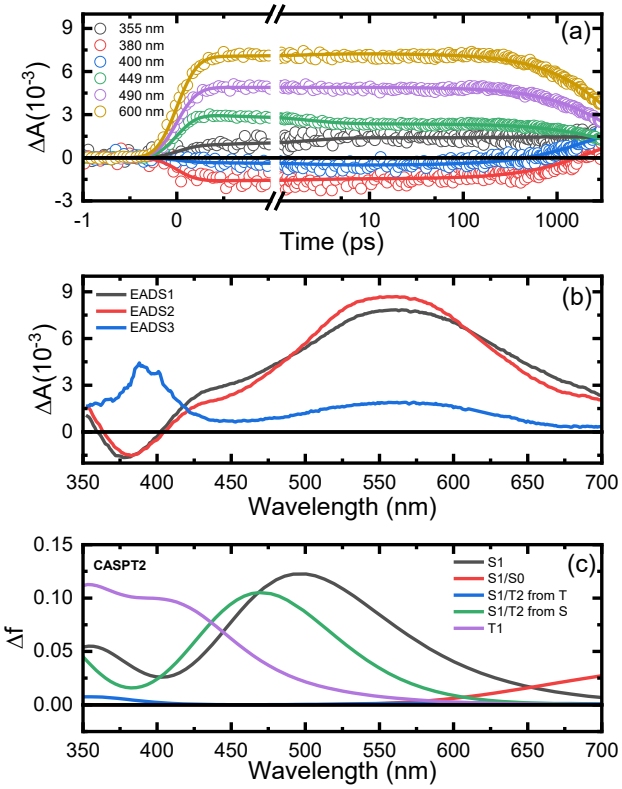

Figure 3. (a) Representative kinetic decay traces of 2oxoP-r, featuring global and target analyses using a three-component sequential kinetic model. Note that the abscissa is linear until 1 ps, after which a log scale is used. (b) Evolution associated difference spectra (EADS) presented for 2oxoP-r in the 350 to 700 nm region. The spectral region from 320 to 350 nm was not included to avoid fitting the signal from stimulated Raman emission of the solvent. (c) Simulated excited state absorption spectra of the S_{1min}, T_{1min}, $S_1/T_2/T_1$ crossing, and S_1/S_0 conical intersection calculated at the CASPT2 level of theory in vacuum for the N9H 2-oxopurine tautomer.

Quantum chemical calculations

Quantum chemical calculations performed by Corral and coworkers[24] for the N9H 2-oxopurine tautomer in vacuum at the CASPT2 level of theory were used to understand the electronic relaxation pathways of 2oxoP-r. At the Franck Condon (FC) region, MS-CASPT2

predicts that the S_1 state has a ππ* character with an oscillator strength (f) of 0.0903 (3.86 eV), comparable to the results reported by Mburu et al. at the CASSCF/MRMP2 level.[52] The S_2 (nπ*) state is dark (f = 0.0004) and has an energy of 4.97 eV, and should not be populated upon excitation at 308 nm. Minimum energy path calculations for the N9H 2-oxopurine tautomer at the same level of theory describe a barrierless path from the S_1 state in the FC region to the minimum, S_{1min}, with an energy of 3.40 eV (365 nm) above the ground state minimum.[24] A S_1/S_0 conical intersection (CI) was located at 4.03 eV, around 0.6 eV above the S_{1min}; hence, nonradiative decay to the ground state from the S_{1min} is not play a major role in vacuum. It should be noted, however, that ADC(2) and TD-DFT approaches predict a more accessible internal conversion funnel, with an energy only slightly above the one predicted for the S_{1min}. Corral and coworkers also located a $S_1/T_2/T_1$ crossing close to the S_{1min} (3.49 eV) and calculated a significant spin-orbit coupling with the T_2 state of 62 cm^{-1}.[24] Using their nuclear coordinates, simulations of the absorption spectra have for the S_{1min}, T_{1min}, $S_1/T_2/T_1$ crossing, and S_1/S_0 conical intersection of the N9H 2-oxopurine tautomer have been performed in this study, calculated at the CASPT2 level of theory in vacuum (Figure 3c).

Laser flash photolysis and singlet oxygen quantum yields

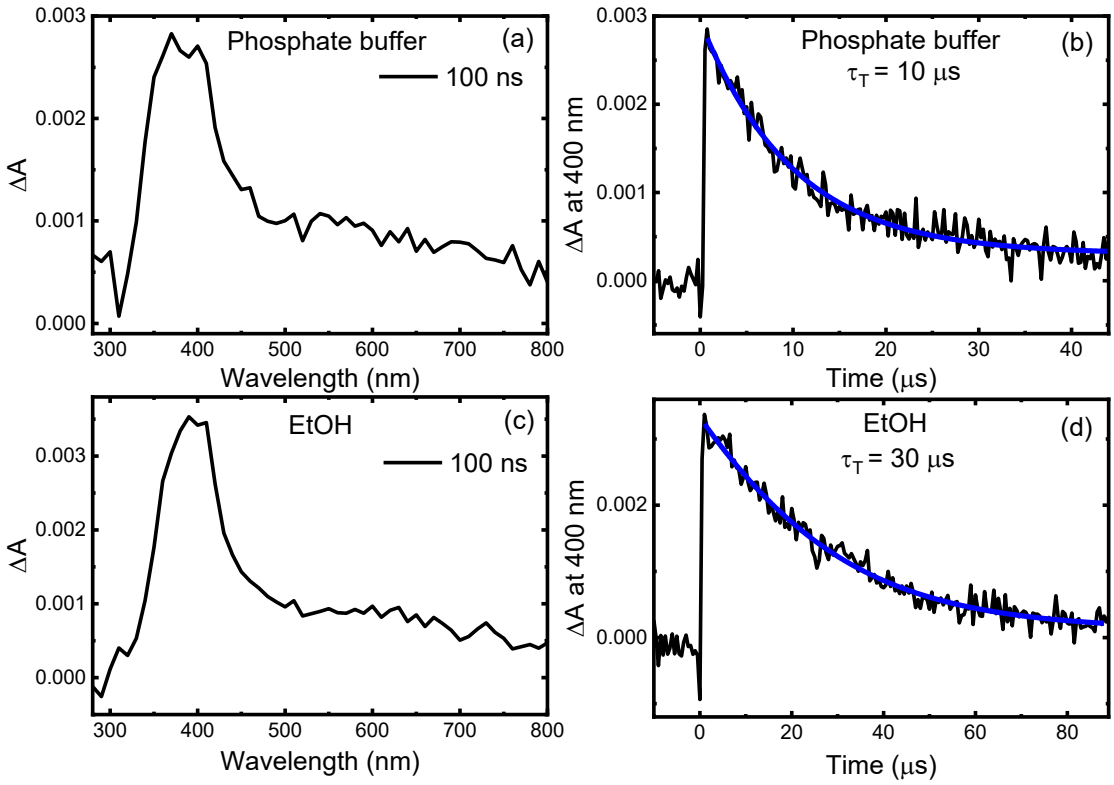

Figure 4. Transient absorption spectra of 2oxoP-r triplet states after pulsed laser excitation at 266 nm (delay 100 ns, gate width 3μs) of argon purged phosphate buffer solutions (16 mM, pH = 6) (a) or ethanol (EtOH) solutions (c) of 2oxoP-r. Corresponding triplet absorbance decay traces monitored at 400 nm are shown in (b) and (d).

Laser flash photolysis experiments were performed to characterize the triplet state of 2oxoP-r in both phosphate buffer and in ethanol (EtOH). The transient absorption spectrum of the triplet state of 2oxoP-r was recorded after pulsed laser excitation at 266 nm. The solutions of 2oxoP-r in both solvents were purged with argon to measure the triplet-triplet absorption spectra

(Figures 4a and c, respectively). The triplet decay traces for 2oxoP-r are presented in Figure 4b in phosphate buffer at pH 6 and in Figure 4d in EtOH. Triplet decay lifetimes of τ_T = 10 μs and τ_T = 30 μs were obtained in phosphate buffer at pH 6 and in EtOH, respectively.

In addition, time-resolved luminescence spectroscopy was used to measure the singlet oxygen quantum yield (Φ_Δ) of 2oxoP-r in both solvents. Figure 5 shows the singlet oxygen phosphorescence measurements for singlet oxygen quantum yield determination for 2oxoP-r in EtOH and in phosphate buffer at pH 6 (Figure 5a and b, respectively). A 10% singlet oxygen quantum yield was obtained for 2oxoP-r in both solvents. The triplet lifetimes and singlet oxygen quantum yields of 2oxoP-r are collected in Table 1.

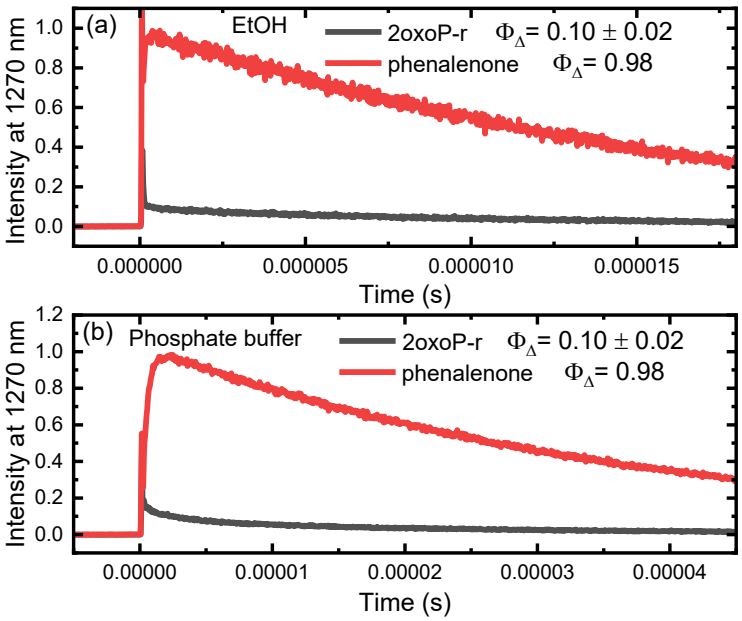

Figure 5. Singlet oxygen phosphorescence decay traces monitored at 1270 nm generated by pulsed photoexcitation (266 nm) of 2oxoP-r or phenalenone in O_2-saturated ethanol (a) and O_2-saturated D_2O buffer solution (phosphate 10 mM, pH = 6) (b).

Table 1. Singlet oxygen quantum yields and triplet lifetimes of 2oxoP-r

Solvent	*EtOH*	*Phosphate buffer*
Φ_Δ *(O_2-saturated)*	0.10 ± 0.02	0.10 ± 0.02[a]
Φ_Δ *(air-saturated)*	0.10 ± 0.02	0.09 ± 0.02[a]
τ_T *(μs) (Ar-saturated)*	30 μs	10 μs[b]

[a] D_2O/phosphate buffer, pH 6

[b] phosphate buffer, pH 6

Discussion

Based on our experimental measurements and the computational results for the N9H 2-oxopurine tautomer,[24] we can propose a deactivation mechanism for 2oxoP-r in phosphate buffer at pH 6 (Scheme 2). Excitation at 308 nm initially populates the S_1 (ππ*) state in the FC region with excess vibrational energy, from where the population traverses to the S_{1min} after conformational and solvent dynamics. Hence, we propose that 1.9 ± 0.4 ps corresponds to both inter- (solvent-solute) and intramolecular vibrational relaxation from the initially populated S_1 (ππ*) state to its minimum, where solvation dynamics is the rate-limiting step. This assignment is supported by the observation of an initial blueshift and band narrowing in the spectral region from ca. 400 to 700 nm (Figures 2a and b), a redshift in the stimulated emission band (Figure 2b), and by the agreement of the absorption spectrum of the S_{1min} shown in Figure 3c with the black EADS1 in Figure 3b. We note that the quantum chemical calculations for the S_{1min} of N9H 2-oxopurine predict the stretching of the C_2-O and N_3-C_4 bonds and a reinforcement of the C_2-N_3 bond relative

to the ground state geometry.[24] Therefore, the black EADS1 in Figure 3b is associated with the excited state absorption of the S_1 ($\pi\pi^*$) state near its minimum.

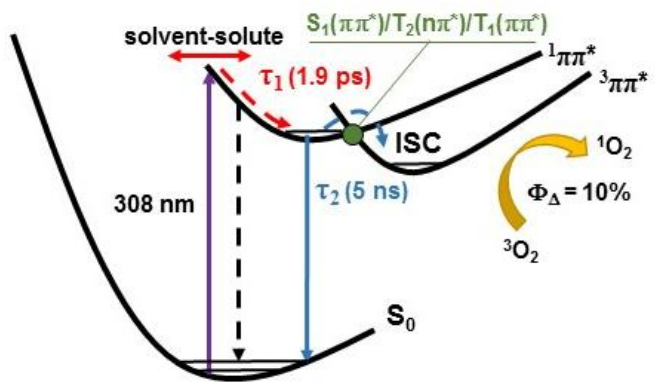

Scheme 2. Proposed excited state relaxation mechanism of 2oxoP-r in phosphate buffer at pH 6. The green circle represents the $S_1/T_2/T_1$ crossing point with a spin-orbit coupling of 62 cm^{-1} reported by Corral and coworkers for the N9H 2oxoP tautomer in vacuum.[24] Inter- and intramolecular vibrational relaxation competes with nonradiative decay to the ground state through a S_1/S_0 conical intersection (not shown)[24] and intersystem crossing to the T_1 state that can sensitize singlet oxygen in a 10% yield.

The steady-state fluorescence yield shows that 48% of the population trapped in the S_{1min} decays by fluorescence, while the time-resolved luminescence experiments demonstrate the generation of singlet oxygen with a quantum yield of 10% (Table 1). In addition, Figure 2c shows a slight increase in intensity of the transient absorption band with maximum at 555 nm for up to ca. 165 ps, which is associated with the red EADS2 shown in Figure 3b. We assign this relaxation process to a bifurcation of the population trapped in the S_{1min} that is either decaying by fluorescence emission (48%) or intersystem crossing to the triplet manifold through a $S_1/T_2/T_1$ crossing region located by Corral and coworkers.[24] As shown in Figure 3c, both the S_{1min} and the $S_1/T_2/T_1$ crossing

absorb in the UV and visible regions according to CASPT2 calculations. The population crossing the $S_1/T_2/T_1$ crossing region internally converts to the T_1 state. This process is associated with the observation of a new absorption band around 380 nm in Figure 2c and Figure 4a,c, while the band with maximum at 555 nm continues to decay for a time delay longer than 3 ns. The calculated absorption spectrum for the T_{1min} shown in Figure 3c supports the assignment of the absorption band at 380 nm to the triplet state. Hence, we assign the lifetime of 5 ± 2 ns to a competition between fluorescence emission from the $^1\pi\pi^*$ state minimum and intersystem crossing to the triplet manifold. The residual transient absorption signal absorbing both in the UV and visible regions, and associated with the blue EADS3 in Figure 3b, is assigned to a linear combination of the absorption spectra of the population still trapped in the S_1 and T_1 minima at 3 ns. This is consistent with the absorption spectrum of the triplet state reported in Figure 4a,c using nanosecond laser flash photolysis, which evidences that the absorption spectrum of the T_1 state has significant absorption intensity around ca. 380 nm with a broad and smaller absorption band that extends above 800 nm and decays back to the ground state in 10 μs in aqueous buffer solution. We were unable to measure the triplet yield because of the lack of a convenient triplet standard; however, the triplet quantum yield can be capped to be between 10% and 52%, according to the fluorescence and singlet oxygen quantum yields in aqueous buffer solution. We also note that according to the calculations for the N9H 2-oxopurine tautomer in vacuum,[24] some of the S_1 population could intersystem cross to the triplet manifold through the $S_1/T_2/T_1$ crossing region on a faster time scale, but given the broad absorption spectra of these species, we cannot unequivocally support or rule this possibility with the experimental and computational data currently in hand.

The excited state population that does not decay by fluorescence emission (48%) or intersystem cross to the triplet state (between 10 to 52%) decays back to the ground state

nonradiatively. The participation of nonradiative decay from the S_1 state to the ground state is in good agreement with the calculations presented by Corral and coworkers for the N9H 2oxoP tautomer,[24] which predict a competition between nonradiative internal conversion to the ground state via a S_1/S_0 conical intersection and intersystem crossing to the triplet state.

Conclusions

2oxoP-r shows promising photophysical properties such as a significant redshifted absorption compared to other isomorphic fluorescent nucleoside analogs,[6] such as 2AP,[35 53 54] 8-vinyl-deoxyadenosine,[55 56] 8-vinyl-2′-deoxyguanosine[57 58] in aqueous solution, and a high fluorescence quantum yield of 48%. The high fluorescence quantum yield positions 2oxoP-r amongst the fluorescent nucleosides currently used as isomorphic fluorescent analogs.[6] Through the combination of steady-state absorption and emission, nanosecond laser flash photolysis, time-resolved IR luminescence, and femtosecond broadband transient absorption spectroscopies, in combination with quantum chemical calculations, the key electronic relaxation pathways for 2oxoP-r in aqueous solution were elucidated, demonstrating that both fluorescence (48%) and nonradiative decay (52%) occur simultaneously in this nucleoside. The nonradiative decay is due to a combination of internal conversion to the ground state and intersystem crossing to the triplet state, with a triplet yield between 10% to 52%. Importantly, the triplet state of 2oxoP-r is long-lived (τ = 10 μs in aqueous solution) and can generate singlet oxygen with a 10% quantum yield. The generation of singlet oxygen by 2oxoP-r is important because it is well-documented that singlet oxygen can damage DNA.[59 60 61 62] Therefore, the experimental results presented in this work demonstrate that 2oxoP-r can be used both as an isomorphic fluorescent analog and as a UVA-photosensitizer in DNA and RNA research.

ASSOCIATED CONTENT

Supporting Information

The Supporting Information is available free of charge on the ACS Publications website at DOI: xxx.

^{1}H NMR spectrum of 2oxoP-r in D_2O at room temperature, FT-IR spectrum of 2oxoP-r neat at room temperature, ground state absorption spectra of 2oxoP-r in phosphate buffer pH 6 before and after 40 minutes of laser irradiation during transient absorption spectroscopy measurements with a dose of 2,546 J cm^{-2} at 308 nm, normalized steady-state absorption, excitation, and emission spectra of 2oxoP-r in phosphate buffer pH 6.

AUTHOR INFORMATION

Corresponding Author

*E-mail: carlos.crespo@case.edu.

Present Address

E.M.A.: Linköping University (Linköping, Sweden), Department of Physics, Chemistry and Biology, Office E308.

Notes

The authors declare no competing financial interests.

Acknowledgment

The authors acknowledge funding from the National Science Foundation (Grant No. CHE-1800052) and thank Dr. Luis A. Ortiz-Rodríguez for his assistance recording the fluorescence quantum yield measurements using the ISS-PC1 photon-counting spectrofluorometer. The authors also thank the Ministerio de Ciencia, Innovación y Universidades of Spain (project PGC2018-094644-B-C21), for financial support, the Ramón y Cajal program and a Formación de Profesorado Universitario contract from the Ministerio de Economía, Industria y Competitividad of Spain. Computational time from the Centro de Computación Científica (CCC) of Universidad Autónoma de Madrid is also gratefully acknowledged.

References

(1) Michailidou, F.; Burnett, D.; Sharma, S. V.; Van Lanen, S. G.; Goss, R. J. M. Natural Products Incorporating Pyrimidine Nucleosides. In *Comprehensive Natural Products III*, Liu, H. W., Begley, T. P. Eds.; Vol. 2; Elsevier, 2020; pp 500-536.
(2) Middleton, C. T.; de La Harpe, K.; Su, C.; Law, Y. K.; Crespo-Hernández, C. E.; Kohler, B. DNA excited-state dynamics: from single bases to the double helix. *Annu. Rev. Phys. Chem.* **2009**, *60*, 217-239.
(3) Crespo-Hernández, C. E.; Cohen, B.; Hare, P. M.; Kohler, B. Ultrafast excited-state dynamics in nucleic acids. *Chem. Rev.* **2004**, *104*, 1977-2019.
(4) Gustavsson, T.; Improta, R.; Markovitsi, D. DNA/RNA: building blocks of life under UV irradiation. *J. Phys. Chem. Lett.* **2010**, *1*, 2025-2030.
(5) Saito, Y.; Suzuki, A.; Saito, I. Fluorescent Purine Nucleosides and Their Applications. In *Modified Nucleic Acids*, Nakatani, K., Tor, Y. Eds.; Springer, Cham, 2016.
(6) Dziuba, D.; Didier, P.; Ciaco, S.; Barth, A.; Seidel, C. A. M.; Mély, Y. Fundamental photophysics of isomorphic and expanded fluorescent nucleoside analogues. *Chem. Soc. Rev.* **2021**, *50*, 7062-7107.
(7) Wilhelmsson, M.; Tor, Y. *Fluorescent Analogues of Biomolecular Building Blocks: Design and Applications: Design and Applications*; John Wiley & Sons, 2016.
(8) Xu, W.; Chan, K. M.; Kool, E. T. Fluorescent nucleobases as tools for studying DNA and RNA. *Nat. Chem* **2017**, *9*, 1043-1055.
(9) Wilson, D. L.; Kool, E. T. Fluorescent Probes of DNA Repair. *ACS Chem. Biol.* **2018**, *13*, 1721-1733.
(10) Tanpure, A. A.; Pawar, M. G.; Srivatsan, S. G. Fluorescent Nucleoside Analogs: Probes for Investigating Nucleic Acid Structure and Function. *Isr. J. Chem.* **2013**, *53*, 366-378.
(11) Brem, R.; Guven, M.; Karran, P. Oxidatively-generated damage to DNA and proteins mediated by photosensitized UVA. *Free Radic. Biol. Med.* **2017**, *107*, 101-109.
(12) Pollum, M.; Ashwood, B.; Jockusch, S.; Lam, M.; Crespo-Hernández, C. E. Unintended Consequences of Expanding the Genetic Alphabet. *J. Am. Chem. Soc.* **2016**, *138* (36), 11457-11460.

(13) Ortiz-Rodríguez, L. A.; Crespo-Hernández, C. E. Thionated Organic Compounds as Emerging Heavy-Atom-Free Photodynamic Therapy Agents. *Chem. Sci.* **2020**, *11*, 11113-11123.
(14) Ashwood, B.; Pollum, M.; Crespo-Hernández, C. E. Photochemical and Photodynamical Properties of Sulfur-Substituted Nucleic Acid Bases. *Photochem. Photobiol.* **2019**, *95*, 33-58.
(15) Pollum, M.; Minh, L.; Jockusch, S.; Crespo-Hernández, C. E. Dithionated Nucleobases as Effective Photodynamic Agent Against Human Epidermoid Carcinoma Cells. *ChemMedChem* **2018**, *13*, 1044-1050.
(16) Farrell, K. M.; Brister, M. M.; Pittelkow, M.; Sølling, T. I.; Crespo-Hernández, C. E. Heavy-Atom Substituted Nucleobases in Photodynamic Applications: Substitution of Sulfur with Selenium in 6-Thioguanine Induces a Remarkable Increase in the Rate of Triplet Decay in 6-Selenoguanine. *J. Am. Chem. Soc.* **2018**, *140*, 11214-11218.
(17) Pollum, M.; Jockusch, S.; Crespo-Hernández, C. E. 2,4-Dithiothymine as a potent UVA chemotherapeutic agent. *J. Am. Chem. Soc.* **2014**, *136*, 17930-17933.
(18) Reelfs, O.; Karran, P.; Young, A. R. 4-thiothymidine sensitization of DNA to UVA offers potential for a novel photochemotherapy. *Photochem. Photobiol. Sci.* **2012**, *11*, 148-154.
(19) Favre, A.; Saintomé, C.; Fourrey, J.-L.; Clivio, P.; Laugâa, P. Thionucleobases as intrinsic photoaffinity probes of nucleic acid structure and nucleic acid-protein interactions. *J. Photochem. Photobiol. B* **1998**, *42*, 109-124.
(20) Ortiz-Rodríguez, L. A.; Reichardt, C.; Hoehn, S. J.; Jockusch, S.; Crespo-Hernández, C. E. Detection of the thietane precursor in the UVA formation of the DNA 6-4 photoadduct. *Nature Commun.* **2020**, *11*.
(21) Vendrell-Criado, V.; Rodrígues-Muñiz, G. M.; Cuquerella, M. C.; Lhiaubet-Vallet, V.; Miranda, M. A. Photosensitization of DNA by 5-methyl-2-pyrimidone deoxyribonucleoside: (6-4) photoproduct as a possible Trojan horse. *Angew. Chem. Int. Ed.* **2013**, *125*, 6604–6607
(22) Hoehn, S. J.; Caldero-Rodríguez, N. E.; Crespo-Hernández, C. E. Photochemistry of RNA, RNA Monomers, and Plausible Prebiotic Precursors. In *DNA Photodamage: From Light Absorption to Cellular Responses and Skin Cancer*, RSC publishing in Comprehensive Series in Photochemical & Photobiological Sciences, 2022; pp 197-226.
(23) Hud, N. V.; Cafferty, B. J.; Krishnamurthy, R.; Williams, L. D. The origin of RNA and 'My Grandfather's Axe'. *Chem. Biol.* **2013**, *20*, 466-474.
(24) Martínez-Fernández, L.; Arslancan, S.; Ivashchenko, D.; Crespo-Hernández, C. E.; Corral, I. Tracking the origin of photostability in purine nucleobases: the photophysics of 2-oxopurine. *Phys. Chem. Chem. Phys.* **2019**, *21*, 13467-13473.
(25) Holý, A. Preparation of 9-(β-D-Ribofuranosyl)-2-Hydroxypurine. *Collection Czechoslov. Chem. Commun.* **1979**, *44*, 2846-2853.
(26) Seela, F.; Chen, Y.; Bindig, U.; Kazimierczuk, Z. Synthesis of 2'-Deoxyisoinosine and Related 2'-Deoxyribonucleosides *Helvetica Chimica Acta* **1994**, *77*, 194-202.
(27) Seela, F.; Chen, Y. 2'-Deoxyisoinosine: Synthesis of a highly fluorescent nucleoside and its incorporation into oligonucleotides. *Nucleosides Nucleotides* **1995**, *14*, 863-866.
(28) Seela, F.; Chen, Y. Oligonucleotides containing fluorescent 2'-deoxyisoinosine: solid-phase synthesis and duplex stability. *Nucleic Acids Research* **1995**, *23*, 2499-2505.
(29) Raux, B.; Voitovich, Y.; Derviaux, C.; Lugari, A.; Rebuffet, E.; Milhas, S.; Priet, S.; Roux, T.; Trinquet, E.; Guillemot, J. C.; et al. Exploring Selective Inhibition of the First Bromodomain of the Human Bromodomain and Extra-terminal Domain (BET) Proteins. *J. Med. Chem.* **2016**, *59*, 1634-1641.

(30) Gottlieb, H. E.; Kotlyar, V.; Nudelman, A. NMR Chemical Shifts of Common Laboratory Solvents as Trace Impurities. *J. Org. Chem.* **1997**, *62*, 7512-7515.
(31) Babij, N. R.; McCusker, E. O.; Whiteker, G. T.; Canturk, B.; Choy, N.; Creemer, L. C.; De Amicis, C. V.; Hewlett, N. M.; Johnson, P. L.; Knobelsdorf, J. A., et al. NMR Chemical Shifts of Trace Impurities: Industrially Preferred Solvents Used in Process and Green Chemistry. *Org. Process Res. Dev.* **2016**, *20*, 661-667.
(32) *Gaussian 16, Revision C.01*; Gaussian, Inc.: Wallingford CT., 2016.
(33) Brouwer, A. M. Standards for photoluminescence quantum yield measurements in solution. *Pure Appl. Chem.* **2011**, *83*, 2213-2228.
(34) Reichardt, C.; Vogt, R. A.; Crespo-Hernández, C. E. On the origin of ultrafast nonradiative transitions in nitro-polycyclic aromatic hydrocarbons: excited-state dynamics in 1-nitronaphthalene. *J. Chem. Phys.* **2009**, *131*, 224518.
(35) Reichardt, C.; Wen, C.; Vogt, R.; Crespo-Hernández, C. Role of Intersystem Crossing in the Fluorescence Quenching of 2-Aminopurine 2'-deoxyriboside in Solution. *Photochem. Photobiol. Sci.* **2013**, *12*, 1341-1350.
(36) Snellenburg, J. J.; Laptenok, S.; Seger, R.; Mullen, K. M.; van Stokkum, I. H. M. Glotaran: A Java-Based Graphical User Interface for the R Package TIMP. *J. Stat. Softw.* **2012**, *49* (3), 1-22.
(37) Roos, B. O. *Ab Initio Methods in Quantum Chemistry*; Wiley, 1987.
(38) Hehre, W. J.; Ditchfield, R.; Pople, J. A. Self—Consistent Molecular Orbital Methods. XII. Further Extensions of Gaussian—Type Basis Sets for Use in Molecular Orbital Studies of Organic Molecules. *J. Chem.Phys.* **1972**, *56*, 2257-2261.
(39) Finley, J.; Malmqvist, P.-A.; Roos, B. O.; Serrano-Andrés, L. The multi-state CASPT2 method. *Chem. Phys. Lett.* **1998**, *288*, 299-306.
(40) Dill, J. D.; Pople, J. A. Self- consistent molecular orbital methods. XV. Extended Gaussian- type basis sets for lithium, beryllium, and boron. *J. Chem. Phys.* **1975**, *62*, 2921-2923.
(41) Ghigo, G.; Roos, B. O.; Malmquist, P.-Å. A modified definition of the zeroth-order Hamiltonian in multiconfigurational perturbation theory (CASPT2). *Chem. Phys. Lett.* **2004**, (396), 142-149.
(42) Forsberg, N.; Malmquist, P.-Å. Multiconfiguration perturbation theory with imaginary level shift. *Chem. Phys. Lett.* **1997**, *274*, 196-204.
(43) Galván, I. F.; Vacher, M.; Alavi, A.; Angeli, C.; Aquilante, F.; Autschbach, J.; Bao, J. J.; Bokarev, S. I.; Bogdanov, N. A.; Carlson, R. K.; et al. OpenMolcas: From Source Code to Insight. *J. Chem. Theory Comput.* **2019**, *15* (11), 5925-5964.
(44) Yagci, Y.; Jockusch, S.; Turro, N. J. Mechanism of Photoinduced Step Polymerization of Thiophene by Onium Salts: Reactions of Phenyliodinium and Diphenylsulfinium Radical Cations with Thiophene. *Macromolecules* **2007**, *40*, 4481-4485.
(45) Schmidt, R.; Tanielian, C.; Dunsbach, R.; Wolff, C. Phenalenone, a universal reference compound for the determination of quantum yields of singlet oxygen O_2 ($^1\Delta_g$) sensitization. *J. Photochem. Photobiol. A* **1994**, *79* (1), 11-17.
(46) Mason, S. F. Purine Studies. Part II. The Ultraviolet Absorption Spectra of Some Mono- and Poly-substituted Purines. *J. Chem. Soc.* **1954**, 2071-2081.
(47) Kwiatkowski, J. S. Electronic Spectra of the 2-Oxypurine Isomers *Theoret. Chim. Acta* **1968**, *11*, 167-168.
(48) Albert, A.; Brown, D. J. Purine studies. Part I. Stability to acid and alkali. Solubility. Ionization. Comparison with pteridines. *J. Chem. Soc.* **1954**, 2060-2071.

(49) Fox, J. J.; Van Praag, D. Nucleosides. VIII. Synthesis of 5-Nitrocytidine and Related Nucleosides. *J. Org. Chem.* **1961**, *26*, 526-532.
(50) Po, H. N.; Senozan, N. M. The Henderson–Hasselbalch Equation: Its History and Limitations. *J. Chem. Educ.* **2001**, *78*, 1499-1503.
(51) Serrano-Andrés, L.; Merchán, M.; Borin, A. C. Adenine and 2-aminopurine: paradigms of modern theoretical photochemistry. *Proc. Nat. Acad. Sci. USA* **2006**, *103*, 8691-8696.
(52) Mburu, E.; Matsika, S. An Ab Initio Study of Substituent Effects on the Excited States of Purine Derivatives. *J. Phys. Chem. A* **2008**, *112*, 12485-12491.
(53) Ward, D. C.; Reich, E.; Stryer, L. Fluorescence studies of nucleotides and polynucleotides. I. Formycin, 2-aminopurine riboside, 2,6-diaminopurine riboside, and their derivatives. *J. Biol. Chem.* **1969**, *244* (5), 1228-1237.
(54) Jones, A. C.; Neely, R. K. 2-Aminopurine as a fluorescent probe of DNA conformation and the DNA-enzyme interface. *Q. Rev. Biophys.* **2015**, *48*, 244-279.
(55) Ben Gaied, N.; Glasser, N.; Ramalanjaona, N.; Beltz, H.; Wolff, P.; Marquet, R.; Burger, A.; Mély, Y. 8-vinyl-deoxyadenosine, an alternative fluorescent nucleoside analog to 2'-deoxyribosyl-2-aminopurine with improved properties. *Nucleic Acids Res.* **2005**, *33*, 1031-1039.
(56) Kenfack, C. A.; Piémont, E.; Ben Gaied, N.; Burger, A.; Mély, Y. Time-resolved fluorescent properties of 8-vinyl-deoxyadenosine and 2-amino-deoxyribosylpurine exhibit different sensitivity to their opposite base in duplexes. *J. Phys. Chem. B* **2008**, *112* (32), 9736–9745.
(57) Martínez-Fernández, L.; Gustavsson, T.; Diederichsen, U.; Improta, R. Excited State Dynamics of 8-Vinyldeoxyguanosine in Aqueous Solution Studied by Time-Resolved Fluorescence Spectroscopy and Quantum Mechanical Calculations. *Molecules* **2020**, *25*, 824.
(58) Nadler, A.; Strohmeier, J.; Diederichsen, U. 8-Vinyl-2′-deoxyguanosine as a Fluorescent 2′-Deoxyguanosine Mimic for Investigating DNA Hybridization and Topology. *Angew. Chem., Int. Ed.* **2011**, *50*, 5392–5396.
(59) Cadet, J.; Douki, T. Oxidatively generated damage to DNA by UVA radiation in cells and human skin. *J. Invest. Dermatol.* **2011**, *131*, 1005-1007.
(60) Cadet, J.; Wagner, J. R. DNA Base Damage by Reactive Oxygen Species, Oxidizing Agents, and UV Radiation. *Cold Spring Harb Perspect Biol* **2013**, *5:a012559*.
(61) Cadet, J.; Douki, T.; Ravanat, J. L. Oxidatively Generated Damage to Cellular DNA by UVB and UVA Radiation. *Photochem. Photobiol.* **2015**, *91* (1), 140-155.
(62) Cadet, J.; Douki, T.; Ravanat, J.-L.; Mascio, P. D. Sensitized formation of oxidatively generated damage to cellular DNA by UVA radiation. *Photochem. Photobiol. Sci.* **2009**, *8*, 903-911.

TOC Graphic